Event patterns extracted from top quark-related spectra in proton-proton collisions at 8 TeV

Ya-Hui Chen[1], Fu-Hu Liu[1,*], and Roy A. Lacey[2]
[1] *Institute of Theoretical Physics, Shanxi University, Taiyuan, Shanxi 030006, China*
[2] *Departments of Chemistry & Physics, Stony Brook University, Stony Brook, NY 11794, USA*

arXiv:1611.10150v1 [hep-ph] 30 Nov 2016

Abstract: We analyze the transverse momentum (p_T) and rapidity (y) spectra of top quark pairs, hadronic top quarks, and top quarks produced in proton-proton (pp) collisions at center-of-mass energy $\sqrt{s}$ = 8 TeV. For p_T spectra, we use the superposition of the inverse power-law suggested by the QCD (quantum chromodynamics) calculus and the Erlang distribution resulted from a multisource thermal model. For y spectra, we use the two-component Gaussian function resulted from the revised Landau hydrodynamic model. The modelling results are in agreement with the experimental data measured at the detector level, in the fiducial phase-space, and in the full phase-space by the ATLAS Collaboration at the Large Hadron Collider (LHC). Based on the parameter values extracted from p_T and y spectra, the event patterns in three-dimensional velocity (β_x-β_y-β_z), momentum (p_x-p_y-p_z), and rapidity (y_1-y_2-y) spaces are obtained, and the probability distributions of these components are obtained, too.

Keywords: top quark-related spectra, event pattern, three-dimensional space

PACS: 25.75.Ag, 25.75.Dw, 24.10.Pa

1 Introduction

The top quark is the heaviest particle in the standard model and very different from the other quarks. It is expected that the top quark may have some special characteristics and be related to the new physics beyond the standard model. Therefore, it is very significant to study its characteristics more. The top quark was first found by the Tevatron at the Fermi National Accelerator Laboratory [1–4], and the successful operation of the CERN Large Hadron Collider (LHC) makes the study of the top quark enter a more precise measurement period. High energy collisions are the only way to study the top quark in experiments. Generally, due to the complexity of the process in an extremely short time, theoretical physicists need to use models to analyze the properties of observables instead of to study the interacting systems directly.

Among the kinematic observables, the transverse momentum (p_T) and rapidity (y) are always the hot topics for the theoretical physicists. Some phenomenological models and formulas were proposed to fit the spectra of p_T and y. For p_T spectra, many formulas can be used, such as the standard (Fermi-Dirac, Bose-Einstein, or Boltzmann) distribution [5–8], the Tsallis statistics [8–14], the inverse power-law [15–17], the Erlang distribution [18], the Schwinger mechanism [19–22], and the combination of them, while y spectra can be described by the one-, two-, or three-component Gaussian function. Except for these analytic expressions, many models based on the Monte Carlo method have reported their arithmetic solutions on the spectra of p_T and y, and other interesting results which contain, but are not limited to, chemical and kinetic freeze-out temperatures, chemical potential, transverse flow velocity, particle ratio, and so forth.

In order to understand the sophisticated collision process and mechanism intuitively, we can use the method of event pattern (particle scatter plot) at kinetic freeze-out stage to obtain the information of interaction system. Using this method, we have analyzed the scatter plots of net-baryons produced in central gold-gold (Au-Au) collisions at BNL Relativistic Heavy Ion Collider (RHIC) energies in three-dimensional momentum (p_x-p_y-p_z) space, three-dimensional momentum-rapidity (p_x-p_y-y) space, and three-dimensional velocity (β_x-β_y-β_z) space [23]; charged particles produced in proton-proton (pp) and lead-lead (Pb-Pb) collisions at 2.76 TeV (one of LHC energies) in three-dimensional p_x-p_y-p_z space and β_x-β_y-β_z space [24]; as well as Z bosons and quarkonium states produced in pp and Pb-Pb collisions at LHC energies in two-dimensional transverse

*E-mail: fuhuliu@163.com; fuhuliu@sxu.edu.cn

momentum-rapidity (p_T-y) space and three-dimensional β_x-β_y-β_z space [25]. Due to the variousness of produced particles, further analyses on the event patterns of other particles such as the top quarks are needed.

In this paper, we mainly use the superposition of the inverse power-law suggested by the QCD (quantum chromodynamics) calculus [15–17] and the Erlang distribution resulted from a multisource thermal model [18] and the two-component Gaussian function resulted from the revised Landau hydrodynamic model [26–29] to fit the p_T and y spectra of the top quark-related products produced in pp collisions at the center-of-mass energy $\sqrt{s} = 8$ TeV measured at the detector level, in the fiducial phase-space, and in the full phase-space by the ATLAS Collaboration at the LHC [30]. The related parameters can be extracted from the fitting. Based on the parameters and using the Monte Carlo method, we can obtain the event patterns in three-dimensional β_x-β_y-β_z, p_x-p_y-p_z, and rapidity (y_1-y_2-y) spaces, and the probability distributions of these components can be obtained, too.

The rest part of this paper is structured as followings. A briefly description of the model and method is given in section 2. Then, the results and discussion are presented in section 3. Finally, we summarize our main observations and conclusions in section 4.

2 The model and method

As the heaviest particle in the standard model, the formation of top quark is expected to be through the hard scattering process among partons (quarks and gluons) with high energy. Viewing the top quark-related p_T spectra, one can see a very wide range of distribution. This means that in some cases the spectra can be in fact divided into two parts, one is in the relative high p_T region and mainly contributed by the real hard (the harder) scattering process, and the other one is in the relative low p_T process and mainly contributed by the not too hard (the hard) scattering process.

For the harder and hard processes, we have to choose a superposition distribution which has two components to describe the p_T spectra. In the two components, one is for the harder scattering process and the other one is for the hard scattering process. The relative contributions of the harder scattering process are expected to be different for different products such as the top quark pairs (the $t\bar{t}$ systems), the hadronic top (hadronic t) quarks (the hadronically decaying top quarks), and the top (t) quarks (the semileptonically and hadronically decaying top quarks).

For the harder scattering process, we can use the inverse power-law which is resulted from the QCD calculus [15–17] in high energy collisions to describe the p_T spectra. For the hard scattering process, we can use the Erlang distribution which is resulted from a multisource thermal model [18] to describe the p_T spectra. Although the Erlang distribution is not sure to be the best choice for the hard scattering process, it is a good one to fit many data. In fact, the Erlang distribution is also used for the soft excitation process. The inverse power-law plays a significant role in the region of relative high p_T and the Erlang distribution contributes mainly in the region of relative low p_T.

According to the QCD calculus [15–17], we have the inverse power-law in the form

$$f_1(p_T) = Ap_T\left(1+\frac{p_T}{p_0}\right)^{-n}, \tag{1}$$

where A denotes the normalization constant which makes $\int_0^\infty f_1(p_T)dp_T = 1$, and p_0 and n are free parameters and influence the value of A.

According to the multisource thermal model [18], the spectra of p_T for a given set of data selected in a special condition can be described by the Erlang distribution

$$f_2(p_T) = \frac{p_T^{m-1}}{(m-1)!\langle p_{Ti}\rangle^m}\exp\left(-\frac{p_T}{\langle p_{Ti}\rangle}\right), \tag{2}$$

where $\langle p_{Ti}\rangle$ and m are free parameters. In particular, $\langle p_{Ti}\rangle$ denotes the average value of p_{Ti}, where $i = 1$ to m, and m denotes the number of contribution sources which are in fact the participant partons which contribute the same exponential function to p_T. Generally, $m = 2$ or 3 due to only two or three partons taking part in the formation of each particle.

The top quark-related p_T spectra is a superposition of the inverse power-law and the Erlang distribution. Let k denote the relative contribution of the inverse power-law. Then, the relative contribution of the Erlang distribution is $1-k$. We have the normalized distribution

$$f_0(p_T) = kf_1(p_T) + (1-k)f_2(p_T). \tag{3}$$

In many cases, the spectra of p_T in experiments are presented in terms of non-normalized distribution. To give a comparison with the experimental data, the normalized constant (N_{p_T}) is needed.

According to the Landau hydrodynamic model and its revisions [26–29], we have the y spectrum to be a

Gaussian function [28, 29]

$$f_y(y) = \frac{1}{\sqrt{2\pi}\sigma_y} \exp\left[- \frac{(y-y_C)^2}{2\sigma_y^2} \right], \tag{4}$$

where y_C denotes the mid-rapidity (peak position) and σ_y denotes the distribution width. In the center-of-mass reference frame, $y_C = 0$ corresponds to the symmetric collisions such as the pp collisions considered in the present work.

In many cases, the Gaussian function cannot describe the y spectra very well, we need at least two Gaussian functions for the y spectrum. That is

$$\begin{aligned} f_y(y) = & \frac{k_B}{\sqrt{2\pi}\sigma_{y_B}} \exp\left[- \frac{(y-y_B)^2}{2\sigma_{y_B}^2} \right] \\ & + \frac{1-k_B}{\sqrt{2\pi}\sigma_{y_F}} \exp\left[- \frac{(y-y_F)^2}{2\sigma_{y_F}^2} \right], \end{aligned} \tag{5}$$

where k_B $(1-k_B)$, y_B (y_F), and σ_{y_B} (σ_{y_F}) denote respectively the relative contribution ratio, peak position, and distribution width of the first (second) component which distributes in the backward (forward) rapidity region. Due to the symmetry of pp collisions, we have $k_B = 1 - k_B = 0.5$, $y_B = -y_F$, and $\sigma_{y_B} = \sigma_{y_F}$. When comparing with experimental data, the normalization constant (N_y) is needed.

In the present work, we use the Monte Carlo method to get the discrete values which are used in the event patterns in three-dimensional β_x-β_y-β_z, p_x-p_y-p_z, and y_1-y_2-y spaces. Let R, r_i, and R_{1-5} denote random numbers distributed evenly in $[0, 1]$. To get the discrete values, the variable p_T in Eq. (1) or in the first component in Eq. (3) obeys the following formula

$$\int_0^{p_T} f_1(p_T) dp_T < R < \int_0^{p_T+dp_T} f_1(p_T) dp_T. \tag{6}$$

The variable p_T in Eq. (2) or in the second component in Eq. (3) is obtained by

$$p_T = -\langle p_{Ti} \rangle \sum_{i=1}^{m} \ln r_i = -\langle p_{Ti} \rangle \ln \prod_{i=1}^{m} r_i. \tag{7}$$

As for the variable y in the first and second components in Eq. 5, we have

$$y = \sigma_y \sqrt{-2\ln R_1} \cos(2\pi R_2) + y_B \tag{8}$$

and

$$y = \sigma_y \sqrt{-2\ln R_3} \cos(2\pi R_4) + y_F \tag{9}$$

respectively. An isotropic emission in the transverse plane results in the azimuthal angle φ to be

$$\varphi = 2\pi R_5 \tag{10}$$

which distributes evenly in $[0, 2\pi]$.

In this way, we can get the energy E to be

$$E = \sqrt{p_T^2 + m_0^2} \cosh y, \tag{11}$$

where, m_0 is the peak mass in the invariant mass spectrum of the $t\bar{t}$ systems [30], or the rest mass of top quark in the case of considering the hadronic top quarks or top quarks. The momentum components are

$$p_x = p_T \cos\varphi, \tag{12}$$

$$p_y = p_T \sin\varphi, \tag{13}$$

and

$$p_z = \sqrt{p_T^2 + m_0^2} \sinh y. \tag{14}$$

The velocity components are

$$\beta_x = \frac{p_x}{E}, \tag{15}$$

$$\beta_y = \frac{p_y}{E}, \tag{16}$$

and

$$\beta_z = \frac{p_z}{E}. \tag{17}$$

As for y_1 and y_2, we use the definitions

$$y_1 = \frac{1}{2} \ln\left(\frac{E+p_x}{E-p_x} \right) \tag{18}$$

and

$$y_2 = \frac{1}{2} \ln\left(\frac{E+p_y}{E-p_y} \right) \tag{19}$$

for the rapidities in the directions of ox and oy axes respectively.

In the concrete calculation, we need firstly to fit the p_T and y spectra to get the values of free parameters and normalization constants. Then, we use the values of free parameters obtained by the fitting in the first step to get the discrete values of different kinds of kinematic variables, and repeat for 1000 times to get the event patterns in three-dimensional β_x-β_y-β_z, p_x-p_y-p_z, and y_1-y_2-y spaces. By way of parenthesis, the probability distributions of the velocity, momentum, and rapidity components can be obtained from more discrete values.

3 Results and discussion

Before describing the comparisons with experimental data, we introduce firstly the meanings of "the detector level", "the fiducial phase-space, and "the full phase-space". According to ref. [30] which is quoted in the present work, "the event selection consists of a set of requirements based on the general event quality and

on the reconstructed objects", defined by definite conditions, "that characterize the final-state event topology". Each requirement or condition for quantities of considered event has to be detected, identified, and selected by various types of detectors, which refers to the detector level. The fiducial phase space for the measurements presented in ref. [30] is defined "using a series of requirements applied to particle-level objects close to those used in the selection of the detector-level objects". The full phase space for the measurements presented in ref. [30] is defined "by the set of $t\bar{t}$ pairs in which one top quark decays semileptonically (including τ leptons) and the other decays hadronically".

On the short-cut process of the rest mass for the $t\bar{t}$ systems in the cases of measuring the invariant mass spectra by the three requirements which are (i) at the detector level, (ii) in the fiducial phase-space, and (iii) in the full phase-space, we take $m_0 = 463.2$, 382.5, and 372.5 GeV, respectively, due to the quoted ref. [30]. As for the rest mass of (hadronic) top quark, we take $m_0 = 172.5$ GeV due to the same literature. It is very important to use a correct rest mass in the extraction of event pattern. In the case of giving the spectra of p_T and y, the most important issue is the rest mass.

Figure 1 shows the event yields about (a)(c) p_T and (b)(d) y of (a)(b) the $t\bar{t}$ systems and (c)(d) the hadronic top quarks produced in pp collisions at $\sqrt{s} = 8$ TeV, where y spectra are presented in terms of absolute values. The symbols represent the experimental data of the ATLAS Collaboration [30] measured in the combined electron and muon selections at the detector level, and the error bars are the combined statistical and systematic uncertainties, where the integral luminosity corresponds to 20.3 fb^{-1}. The solid curves are our results calculated by using (a) the inverse power-law, (c) the superposition of the inverse power-law and the Erlang distribution, and (b)(d) the two-component Gaussian distribution, respectively. The dashed curve in (a) is the result calculated by using the Erlang distribution with $m = 1$, which is in fact the exponential distribution for the purpose of comparison. In the calculation, we use the method of least squares to determine the values of parameters. The values of free parameters [p_0, n, k, $\langle p_{Ti}\rangle$, y_F ($= -y_B$), and σ_{y_F} ($= \sigma_{y_B}$)], normalization constants (N_{p_T} and N_y), and χ^2 per degree of freedom (χ^2/dof) are listed in Tables 1–3 for different sets of products and parameters, where $k = 1$ for the $t\bar{t}$ systems and $m = 3$ for the hadronic top quarks.

One can see from Figure 1 and Tables 1–3 that the results calculated by the hybrid model are in agreement with the experimental p_T and y spectra of both the $t\bar{t}$ systems and hadronic top quarks produced in pp collisions at $\sqrt{s} = 8$ TeV measured at the detector level by the ATLAS Collaboration at the LHC. In particular, the $t\bar{t}$ systems show only the contribution of harder scattering process (with $k = 1$), which results in $\langle p_{Ti}\rangle$ and m for the $t\bar{t}$ systems are not available. The hadronic top quarks show mainly the contribution of hard scattering process (with a small k). These render that more collision energies are needed to create the $t\bar{t}$ system. As a part of the $t\bar{t}$ system, the hadronic top quark apportioned partly the energy of $t\bar{t}$ system, which results in a not too hard scattering process.

Figure 2 is the same as that for Figure 1, but it shows the fiducial phase-space normalized differential cross-sections for (a)(b) the $t\bar{t}$ systems and (c)(d) the hadronic top quarks, where σ denotes the cross-section. Figure 3 is also the same as that for Figure 1, but it shows the full phase-space normalized differential cross-sections for (a)(b) the $t\bar{t}$ systems and (c)(d) the top quarks. The corresponding parameters are also listed in Tables 1–3 for different sets of products and parameters, where $k = 1$ for the $t\bar{t}$ systems and $m = 3$ for the hadronic top quarks and top quarks, which are listed only in the captions of Tables 1 and 2, but not in the column.

One can also see from Figures 2 and 3 and Tables 1–3 that the modelling results are in agrement with the experimental data of the fiducial phase-space normalized differential cross-sections for the $t\bar{t}$ systems and the hadronic top quarks, and the full phase-space normalized differential cross-sections for the $t\bar{t}$ systems and the top quarks, produced in pp collisions at 8 TeV measured by the ATLAS Collaboration. In particular, for the $t\bar{t}$ systems in both the fiducial and full phase-spaces, we also have $k = 1$. For both the hadronic top quarks in the fiducial phase-space and the top quarks in the full phase-space, we also have a small k.

As for the tendencies of the free parameters, one can see from Tables 1–3 that, for both the $t\bar{t}$ systems and the (hadronic) top quarks, p_0 and n decrease when the experimental requirement changes from the detector level to the fiducial phase-space and then to the full phase-space. Only for the (hadronic) top quarks, k slightly increases, and $\langle p_{Ti}\rangle$ and m almost do not change when the requirement changes from the detector level to the full phase-space. At the same time, for both the $t\bar{t}$ systems and the (hadronic) top quarks, both y_F and σ_{y_F} increase when the requirement changes from the detector level to the full phase-space. These tendencies may

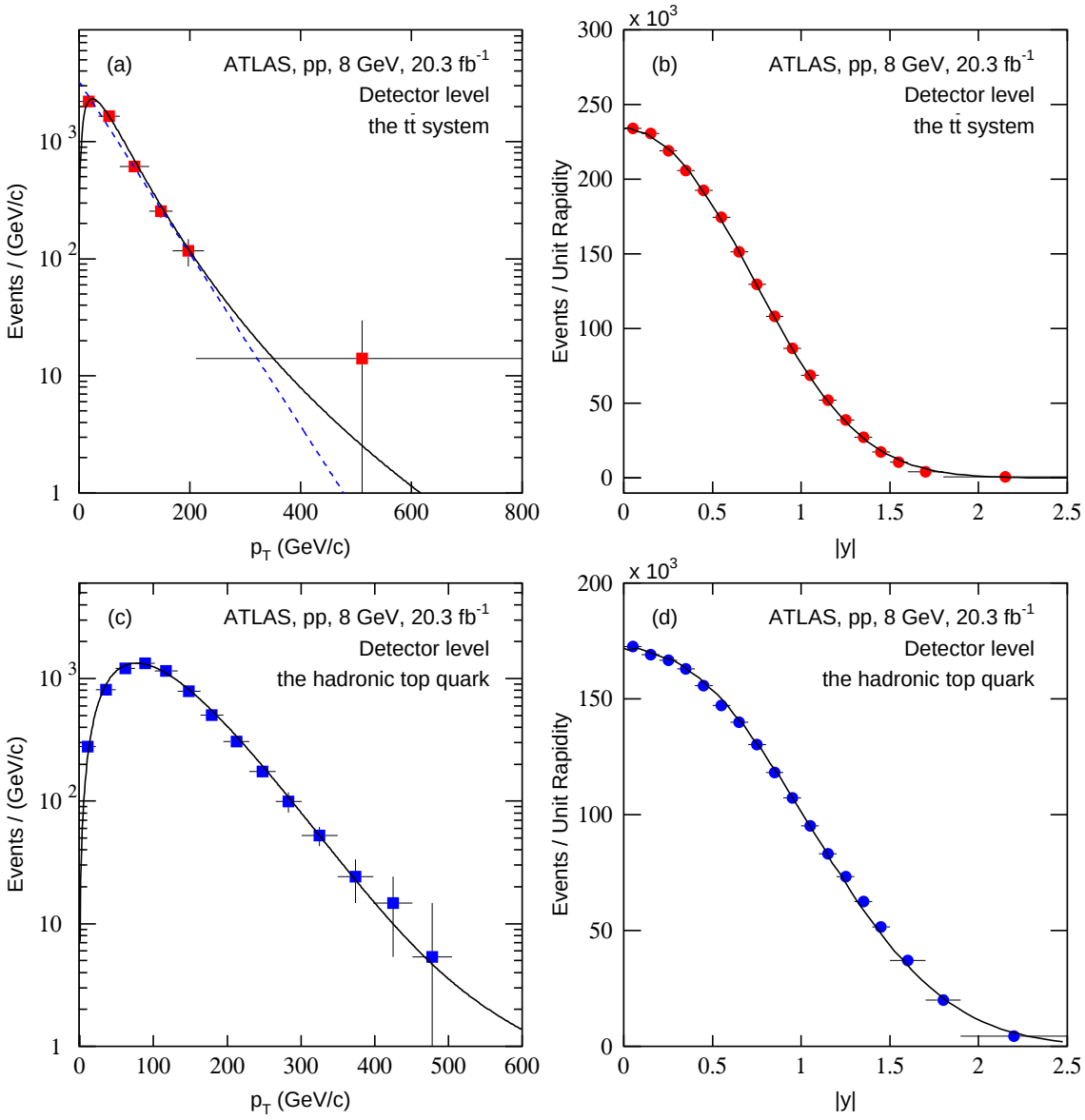

Fig. 1. (a)(c) Transverse momentum and (b)(d) rapidity spectra of (a)(b) the $t\bar{t}$ systems and (c)(d) the hadronic top quarks produced in pp collisions at $\sqrt{s} = 8$ TeV, where the rapidity spectra are presented in terms of absolute values. The symbols represent the experimental data of the ATLAS Collaboration [30] measured in the combined electron and muon selections at the detector level. The solid curves are our results calculated by using the (a) inverse power-law, (c) superposition of inverse power-law and Erlang distribution, and (b)(d) two-component Gaussian distribution, respectively. The dashed curve in (a) is the result calculated by using the Erlang distribution with $m = 1$, which is in fact the exponential distribution.

Table 1. Values of free parameters (p_0 and n), normalization constant (N_{p_T}), and χ^2/dof corresponding to the curves in Figures 1(a), 2(a), and 3(a), where $k = 1$ which results in $\langle p_{Ti} \rangle$ and m are not available.

Figure	Type	p_0 (GeV/c)	n	N_{p_T}	χ^2/dof
Figure 1(a)	$t\bar{t}$	162.86 ± 4.20	7.70 ± 0.40	$(1.93 \pm 0.05) \times 10^5$	2.88
Figure 2(a)	$t\bar{t}$	52.73 ± 2.60	4.34 ± 0.20	1.00	4.26
Figure 3(a)	$t\bar{t}$	45.83 ± 2.50	4.30 ± 0.20	1.00	1.43

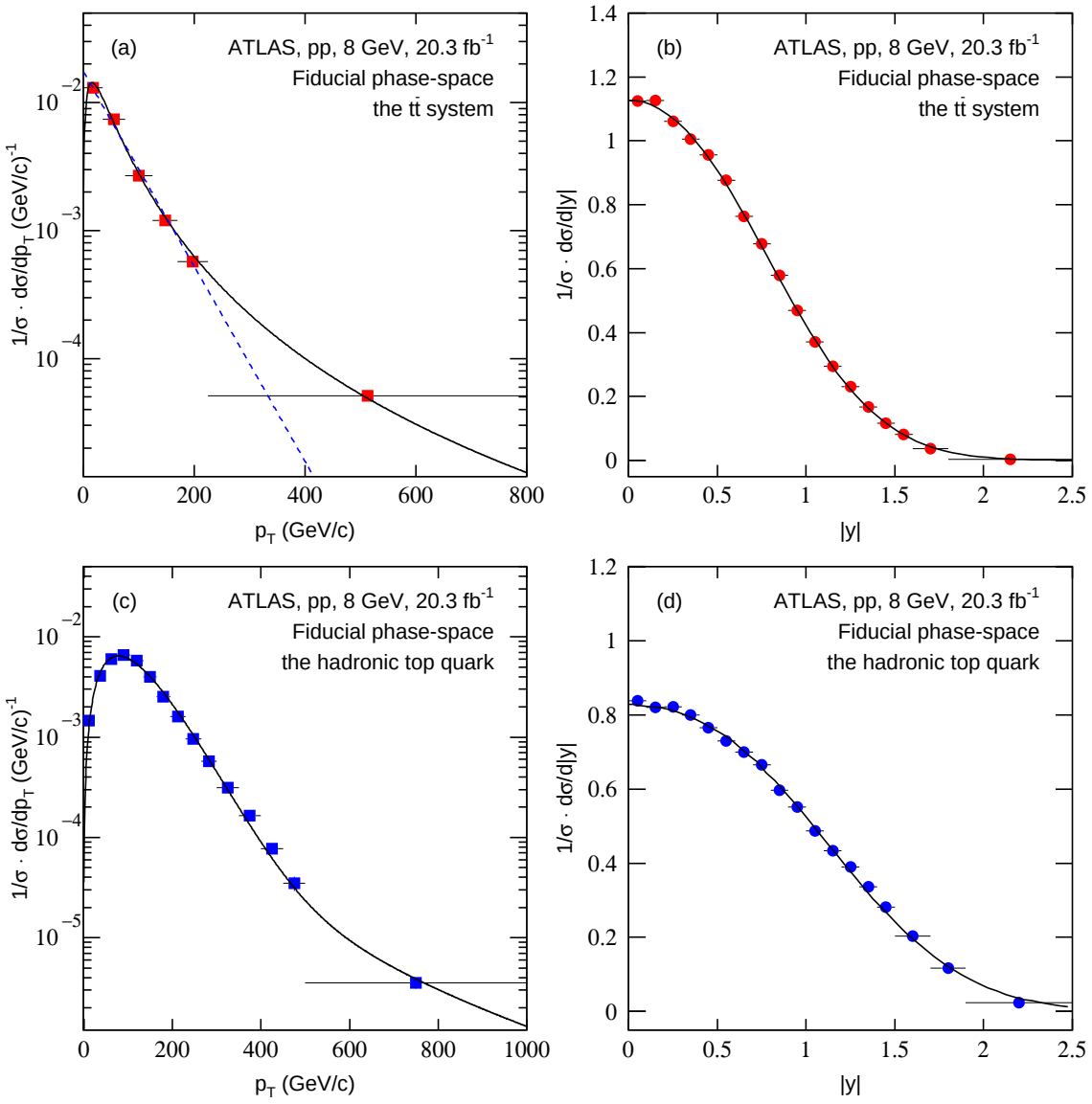

Fig. 2. Same as Figure 1, but showing the fiducial phase-space normalized differential cross-sections.

Table 2. Values of free parameters (p_0, n, k, $\langle p_{Ti}\rangle$, and m), normalization constant (N_{p_T}), and χ^2/dof corresponding to the curves in Figures 1(c), 2(c), and 3(c), where the values of m in the Erlang distribution are invariably taken to be 3 which are not listed in the column.

Figure	Type	p_0 (GeV/c)	n	k	$\langle p_{Ti}\rangle$ (GeV/c)	N_{p_T}	χ^2/dof
Figure 1(c)	hadronic t	225.00 ± 22.50	6.50 ± 1.00	0.10 ± 0.02	39.70 ± 0.50	$(1.99 \pm 0.05) \times 10^5$	11.34
Figure 2(c)	hadronic t	204.00 ± 20.40	6.05 ± 1.00	0.13 ± 0.02	40.50 ± 0.05	1.00	14.33
Figure 3(c)	t	165.00 ± 16.50	5.60 ± 1.00	0.14 ± 0.02	39.20 ± 0.05	1.00	3.76

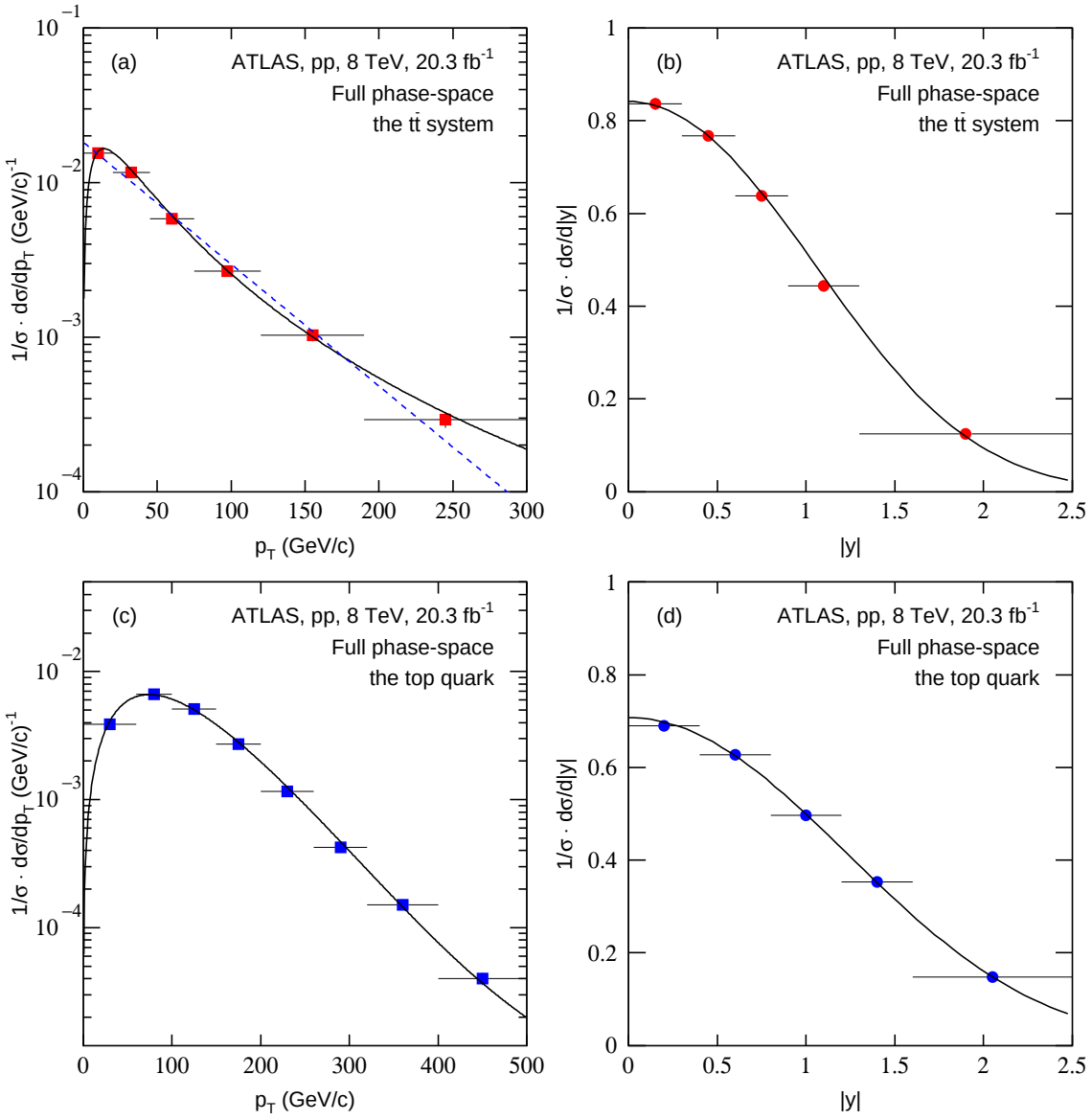

Fig. 3. Same as Figure 1, but showing the full phase-space normalized differential cross-sections for (a)(b) the $t\bar{t}$ systems and (c)(d) the top quarks.

Table 3. Values of free parameter [y_F ($= -y_B$) and σ_{y_F} ($= \sigma_{y_B}$)], normalization constant (N_η), and χ^2/dof corresponding to the curves in Figures 1(b), 1(d), 2(b), 2(d), 3(b), and 3(d).

Figure	Type	y_F ($= -y_B$)	σ_{y_F} ($= \sigma_{y_B}$)	N_y	χ^2/dof
Figure 1(b)	$t\bar{t}$	0.36 ± 0.02	0.53 ± 0.02	$(196.00 \pm 2.00) \times 10^3$	2.27
Figure 1(d)	hadronic t	0.53 ± 0.02	0.68 ± 0.02	$(199.00 \pm 2.00) \times 10^3$	2.21
Figure 2(b)	$t\bar{t}$	0.39 ± 0.02	0.55 ± 0.02	1.00	7.88
Figure 2(d)	hadronic t	0.57 ± 0.02	0.69 ± 0.02	1.01 ± 0.01	13.46
Figure 3(b)	$t\bar{t}$	0.52 ± 0.02	0.79 ± 0.03	1.04 ± 0.01	4.64
Figure 3(d)	t	0.58 ± 0.02	0.98 ± 0.03	1.04 ± 0.01	6.55

Table 4. Values of the root-mean-squares $\sqrt{\overline{\beta_x^2}}$ for β_x, $\sqrt{\overline{\beta_y^2}}$ for β_y, and $\sqrt{\overline{\beta_z^2}}$ for β_z, as well as the maximum $|\beta_x|$, $|\beta_y|$, and $|\beta_z|$ ($|\beta_x|_{\max}$, $|\beta_y|_{\max}$, and $|\beta_z|_{\max}$) corresponding to the scatter plots for different types of products, where the corresponding scatter plots are presented in Figure 4. Both the root-mean-squares and the maximum velocity components are in the units of c.

Figure	Type	$\sqrt{\overline{\beta_x^2}}$	$\sqrt{\overline{\beta_y^2}}$	$\sqrt{\overline{\beta_z^2}}$	$\|\beta_x\|_{\max}$	$\|\beta_y\|_{\max}$	$\|\beta_z\|_{\max}$
Figure 4(a)	$t\bar{t}$	0.11 ± 0.01	0.11 ± 0.01	0.50 ± 0.01	0.58	0.56	0.96
Figure 4(b)	hadronic t	0.31 ± 0.01	0.32 ± 0.01	0.59 ± 0.01	0.79	0.82	0.99
Figure 4(c)	$t\bar{t}$	0.13 ± 0.01	0.14 ± 0.01	0.52 ± 0.01	0.76	0.67	0.97
Figure 4(d)	hadronic t	0.31 ± 0.01	0.32 ± 0.01	0.61 ± 0.01	0.81	0.87	0.99
Figure 4(e)	$t\bar{t}$	0.10 ± 0.01	0.10 ± 0.01	0.62 ± 0.01	0.52	0.46	0.99
Figure 4(f)	t	0.28 ± 0.01	0.29 ± 0.01	0.67 ± 0.01	0.77	0.84	1.00

have no obvious meaning due to little relations among these requirements. However, because these tendencies, we can obtain abundant structures of event patterns.

Based on the parameter values obtained from Figures 1–3 and listed in Tables 1–3, the Monte Carlo calculation can be performed and the values of a series of kinematical quantities can be obtained. Thus, we can get different kinds of diagrammatic sketches at the kinetic freeze-out of the interacting system formed in pp collisions. Figures 4–6 give the event patterns which are displayed by the particle scatter plots in the three-dimensional β_x-β_y-β_z, p_x-p_y-p_z, and y_1-y_2-y spaces, respectively. In these figures, panels (a)–(f) correspond to the results for the $t\bar{t}$ systems at the detector level, the hadronic top quarks at the detector level, the $t\bar{t}$ systems in the fiducial phase-space, the hadronic top quarks in the fiducial phase-space, the $t\bar{t}$ systems in the full phase-space, and the top quarks in the full phase-space, respectively. The total number of particles for each panel is 1000. The blue and red globules represent the contributions of inverse power-law and Erlang distribution respectively. The values of root-mean-squares ($\sqrt{\overline{\beta_x^2}}$ for β_x, $\sqrt{\overline{\beta_y^2}}$ for β_y, and $\sqrt{\overline{\beta_z^2}}$ for β_z,) and the maximum $|\beta_x|$, $|\beta_y|$, and $|\beta_z|$ ($|\beta_x|_{\max}$, $|\beta_y|_{\max}$, and $|\beta_z|_{\max}$) are listed in Table 4. The values of root-mean-squares ($\sqrt{\overline{p_x^2}}$ for p_x, $\sqrt{\overline{p_y^2}}$ for p_y, and $\sqrt{\overline{p_z^2}}$ for p_z), and the maximum $|p_x|$, $|p_y|$, and $|p_z|$ ($|p_x|_{\max}$, $|p_y|_{\max}$, and $|p_z|_{\max}$) are listed in Table 5. The values of root-mean-squares ($\sqrt{\overline{y_1^2}}$ for y_1 and $\sqrt{\overline{y_2^2}}$ for y_2) and the maximum $|y_1|$ and $|y_2|$ ($|y_1|_{\max}$ and $|y_2|_{\max}$) are listed in Table 6. The values of these kinematical quantities listed in Tables 4–6 are obtained by higher statistics.

From Figures 4–6 and Tables 4–6, one can see that the event patterns in the three-dimensional β_x-β_y-β_z space for the $t\bar{t}$ systems in the three requirements are rough cylinders with $\sqrt{\overline{\beta_x^2}} \approx \sqrt{\overline{\beta_y^2}} \ll \sqrt{\overline{\beta_z^2}}$ and $|\beta_x|_{\max} \approx |\beta_y|_{\max} < |\beta_z|_{\max}$, though little differences among the three requirements are observed. The event patterns for the (hadronic) top quarks in the three requirements are rough ellipsoids with the similar relations among these quantities and little differences among the three requirements. An obvious difference between the event patterns for the $t\bar{t}$ systems and the (hadronic) top quarks are observed due to their different production processes. Meanwhile, both the quantities on the root-mean-squares and the maximums for the $t\bar{t}$ systems are less than those for the (hadronic) top quarks, and the differences in relative sizes between transverse and longitudinal quantities for the $t\bar{t}$ systems are larger than those for the (hadronic) top quarks.

The event patterns in the three-dimensional p_x-p_y-p_z space for the $t\bar{t}$ systems in the three requirements are relative thin and very rough ellipsoids with $\sqrt{\overline{p_x^2}} \approx \sqrt{\overline{p_y^2}} \ll \sqrt{\overline{p_z^2}}$ and $|p_x|_{\max} \approx |p_y|_{\max} \ll |p_z|_{\max}$, though little differences among the three requirements are observed. The event patterns for the (hadronic) top quarks in the three requirements are relative fat and very rough ellipsoids with the similar relations among these quantities and little differences among the three requirements. An obvious difference between the event patterns for the $t\bar{t}$ systems and the (hadronic) top quarks are observed. Meanwhile, the transverse quantities for the $t\bar{t}$ systems are less than those for the (hadronic) top quarks, and the situations of longitudinal quantities are opposite. The differences in relative sizes between transverse and longitudinal quantities for the $t\bar{t}$ systems are larger than those for the (hadronic) top quarks. The maximum quantities do not show an obvious tendency for the $t\bar{t}$ systems and the (hadronic) top quarks.

The event patterns in the three-dimensional y_1-y_2-y space for the $t\bar{t}$ systems in the three requirements are very rough ellipsoids with $\sqrt{\overline{y_1^2}} \approx \sqrt{\overline{y_2^2}} \ll \sqrt{\overline{y^2}}$ and $|y_1|_{\max} \approx |y_2|_{\max} \ll |y|_{\max}$, though little differences among the three requirements are observed. The event patterns for the (hadronic) top quarks in the three requirements are very rough rhombogen with the similar relations among these quantities and little differences among the three requirements. An obvious difference

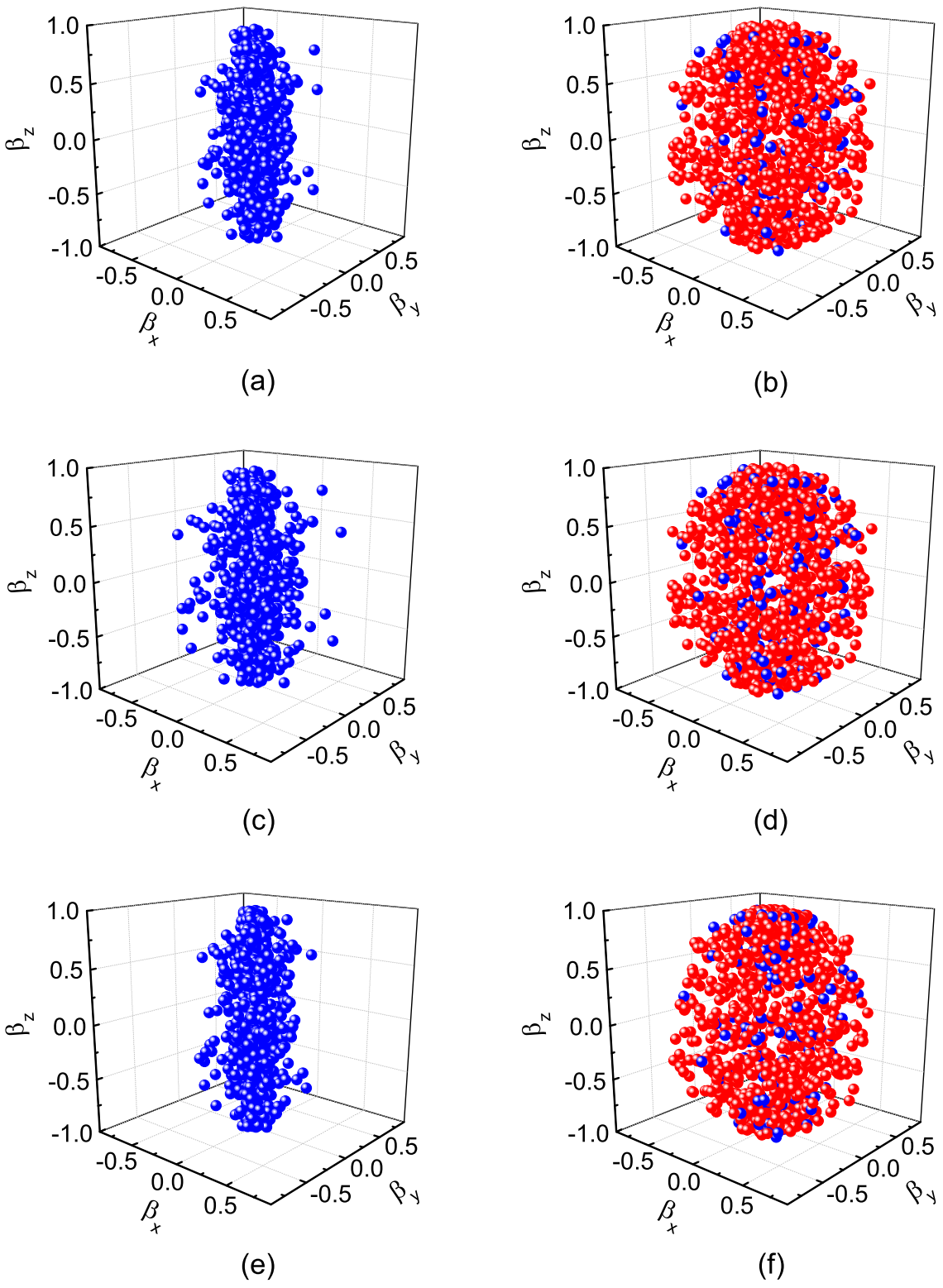

Fig. 4. Event patterns (particle scatter plots) in three-dimensional β_x-β_y-β_z space in pp collisions at $\sqrt{s} = 8$ TeV (a)(b) at the detector level, (c)(d) in the fiducial phase-space, and (e)(f) in the full phase-space, for (a)(c)(e) the $t\bar{t}$ systems, (b)(d) the hadronic top quarks, and (f) the top quarks. The number of particles for each panel is 1000. The blue and red globules represent the results corresponding to the inverse power-law function and the Erlang distribution for p_T, respectively.

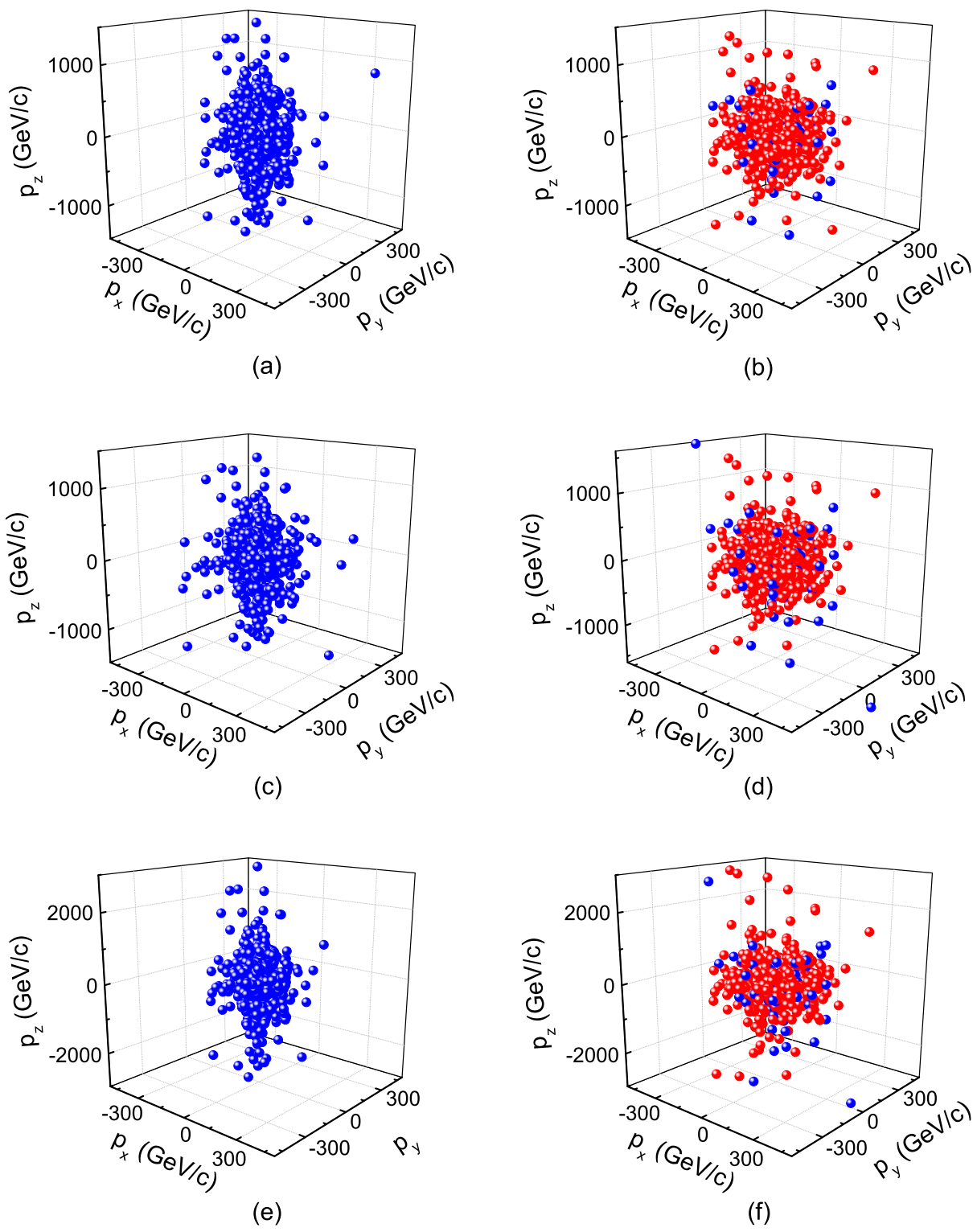

Fig. 5. Same as Figure 4, but showing the results in three-dimensional p_x-p_y-p_z space.

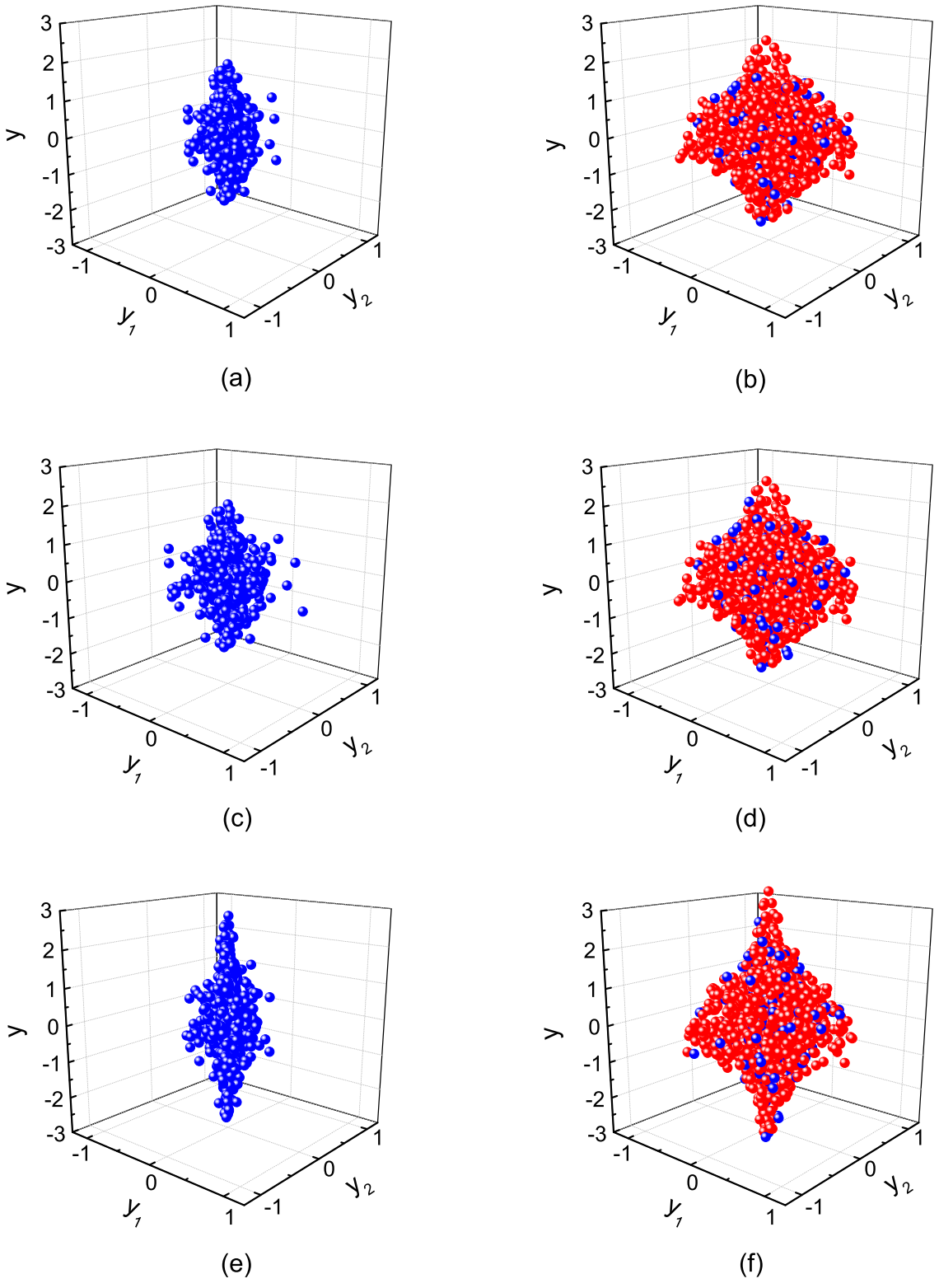

Fig. 6. Same as Figure 4, but showing the results in three-dimensional y_1-y_2-y space.

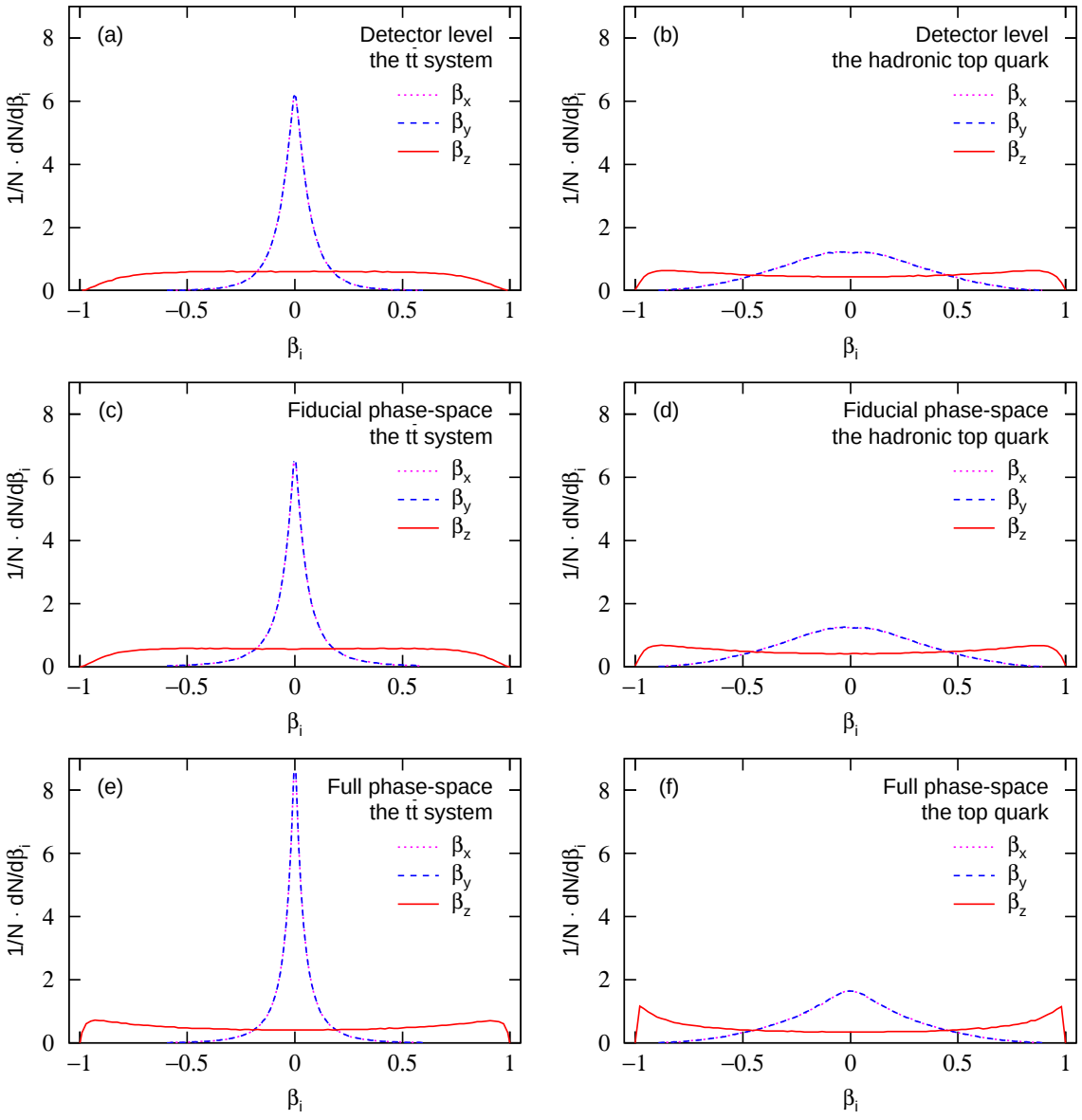

Fig. 7. Distributions of velocity components β_x, β_y, and β_z in pp collisions at $\sqrt{s} = 8$ TeV (a)(b) at the detector level, (c)(d) in the fiducial phase-space, and (e)(f) in the full phase-space, for (a)(c)(e) the $t\bar{t}$ systems, (b)(d) the hadronic top quarks, and (f) the top quarks. The dotted, dashed, and solid curves correspond to the distributions of β_x, β_y, and β_z, respectively, where the distributions of β_x and β_y are nearly the same.

Table 5. Values of the root-mean-squares $\sqrt{\overline{p_x^2}}$ for p_x, $\sqrt{\overline{p_y^2}}$ for p_y, and $\sqrt{\overline{p_z^2}}$ for p_z, as well as the maximum $|p_x|$, $|p_y|$, and $|p_z|$ ($|p_x|_{\max}$, $|p_y|_{\max}$, and $|p_z|_{\max}$) corresponding to the scatter plots for different types of products, where the corresponding scatter plots are presented in Figure 5. Both the root-mean-squares and maximum momentum components are in the units of GeV/c.

Figure	Type	$\sqrt{\overline{p_x^2}}$	$\sqrt{\overline{p_y^2}}$	$\sqrt{\overline{p_z^2}}$	$\lvert p_x\rvert_{\max}$	$\lvert p_y\rvert_{\max}$	$\lvert p_z\rvert_{\max}$
Figure 5(a)	$t\bar{t}$	63.2 ± 2.8	63.9 ± 2.8	373.4 ± 11.0	427.4	469.0	1545.0
Figure 5(b)	hadronic t	97.0 ± 2.7	98.8 ± 2.5	279.1 ± 10.8	433.6	384.8	1347.2
Figure 5(c)	$t\bar{t}$	75.1 ± 4.7	74.9 ± 4.4	338.2 ± 10.3	589.3	632.2	1399.1
Figure 5(d)	hadronic t	100.9 ± 3.1	102.8 ± 3.0	304.9 ± 13.4	498.6	560.5	1999.9
Figure 5(e)	$t\bar{t}$	52.4 ± 2.1	53.2 ± 2.0	574.6 ± 23.7	273.5	255.6	3189.3
Figure 5(f)	t	95.0 ± 2.6	96.8 ± 2.5	513.9 ± 28.8	393.8	423.9	3079.7

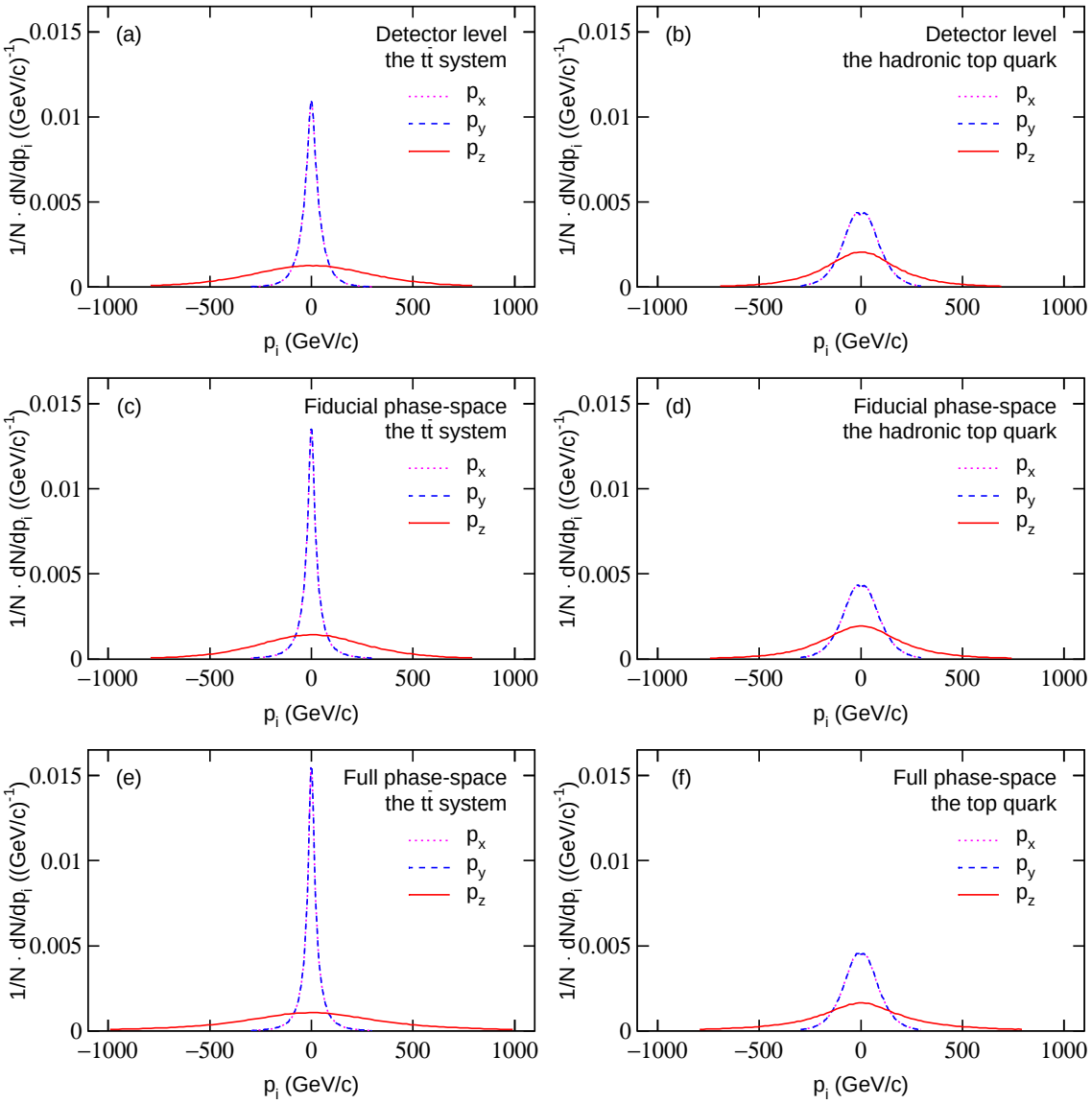

Fig. 8. Same as Figure 7, but showing the distributions of momentum components p_x, p_y, and p_z.

Table 6. Values of the root-mean-squares $\sqrt{\overline{y_1^2}}$ for y_1, $\sqrt{\overline{y_2^2}}$ for y_2, and $\sqrt{\overline{y^2}}$ for y, as well as the maximum $|y_1|$, $|y_2|$, and $|y|$ ($|y_1|_{\max}$, $|y_2|_{\max}$, and $|y|_{\max}$) corresponding to the scatter plots for different types of products, where the corresponding scatter plots are presented in Figure 6.

Figure	Type	$\sqrt{\overline{y_1^2}}$	$\sqrt{\overline{y_2^2}}$	$\sqrt{\overline{y^2}}$	$\lvert y_1\rvert_{\max}$	$\lvert y_2\rvert_{\max}$	$\lvert y\rvert_{\max}$
Figure 6(a)	$t\bar{t}$	0.11 ± 0.01	0.11 ± 0.01	0.65 ± 0.01	0.67	0.63	1.92
Figure 6(b)	hadronic t	0.34 ± 0.01	0.36 ± 0.01	0.87 ± 0.02	1.08	1.16	2.53
Figure 6(c)	$t\bar{t}$	0.14 ± 0.01	0.15 ± 0.01	0.68 ± 0.01	1.01	0.81	2.01
Figure 6(d)	hadronic t	0.34 ± 0.01	0.36 ± 0.01	0.90 ± 0.02	1.12	1.34	2.60
Figure 6(e)	$t\bar{t}$	0.10 ± 0.01	0.11 ± 0.01	0.95 ± 0.02	0.58	0.49	2.84
Figure 6(f)	t	0.30 ± 0.01	0.33 ± 0.01	1.15 ± 0.03	1.02	1.22	3.46

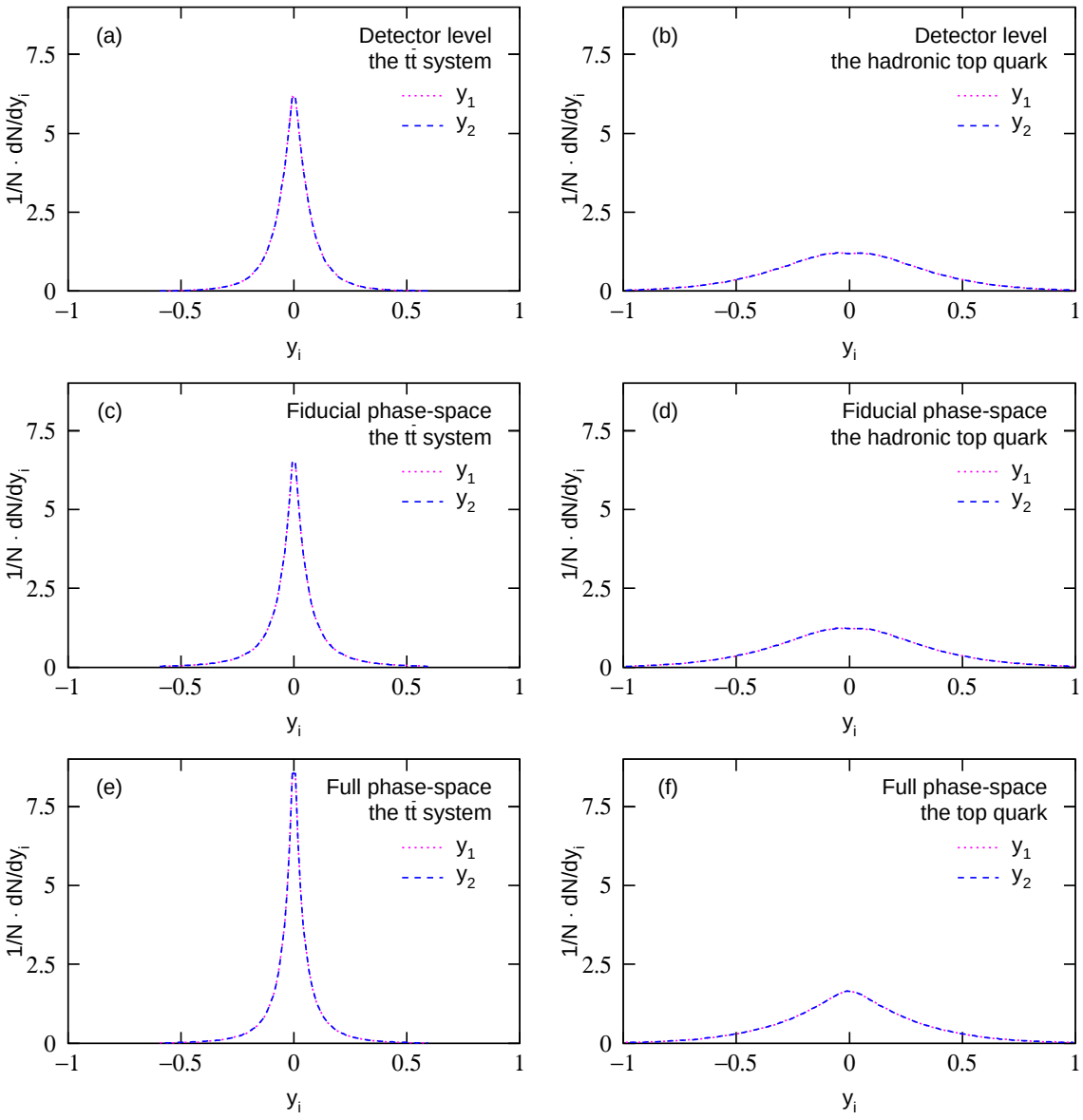

Fig. 9. Same as Figure 7, but showing only the distributions of y_1 and y_2.

between the event patterns for the $t\bar{t}$ systems and the (hadronic) top quarks are observed. Meanwhile, both the quantities on the root-mean-squares and the maximums for the $t\bar{t}$ systems are obviously less than those for the (hadronic) top quarks. The differences in relative sizes between transverse and longitudinal quantities for the $t\bar{t}$ systems are larger than those for the (hadronic) top quarks.

According to these scatter plots (Figures 4–6), we can obtain the probability distributions of the considered quantities. Using higher statistics, Figures 7–9 present the probability distributions of β_i ($i = x$, y, and z), p_i ($i = x$, y, and z), and y_i ($i = 1$ and 2), respectively, where N denotes the number of particles. Different panels correspond to different requirements and different curves correspond to different quantities shown in the panels. One can see that the distributions of x and y components are almost the same, if not equal to each other at the pixel level, due to the assumption of isotropic emission in the transverse plane. All distributions of x, y and z components are symmetric at zero.

On the velocity components, β_x and β_y distribute only in a small region near zero. The $t\bar{t}$ systems have a more narrow region and a higher peak than the (hadronic) top quarks. For the requirements from the detector level to the fiducial phase-space then to the full phase-space, the peak value increases obviously. β_z distributes almost uniformly in a wide region for different particles and requirements. In particular, the distributions of $|\beta_z|$ of the (hadronic) top quarks increase slightly with the increase of $|\beta_z|$, while the $t\bar{t}$ systems show an opposite or placid tendency. Moreover, the tendency in the full phase-space is more obvious than those in the fiducial phase-space and at the detector level. The main differences appear near $|\beta_z|_{\max}$ and are caused by different m_0.

On the momentum components, all the distributions of p_x, p_y, and p_z for different particles and requirements have a peak at zero, though the distribution of p_z has a wider range and a lower peak than those of p_x and p_y. The $t\bar{t}$ systems have a higher and higher peak in p_x and p_y distributions in proper order at the detector level, in the fiducial phase-space, and in the full phase-space, while other three types of distributions have severally similar shapes and do not show obviously the tendency of higher and higher peak.

As for the distributions of y_1 and y_2, one can see a higher and higher peak for the $t\bar{t}$ systems for the requirements from the detector level to the fiducial phase-space then to the full phase-space. For the hadronic top quarks, the distributions of y_1 and y_2 at the detector level and in the fiducial phase-space are almost the same, and they are different in shape and slope around the peak region from the distributions for the top quarks.

For comparisons with our recent works [23–25], as an example, we can see the similarity and difference in the three-dimensional β_x-β_y-β_z space. The scatter plots of $t\bar{t}$ systems and (hadronic) top quarks are similar to those of Z bosons and quarkonium states [25] due to they being heavy particles. In fact, the scatter plots of heavy particles show that the root-mean square velocities form a rough cylinder or ellipsoid surface and the maximum velocities form a fat cylinder or ellipsoid surface, due to their productions being at the initial stage of collisions. The scatter plots of charged particles show that the root-mean-square velocities form an ellipsoid surface and the maximum velocities form a spherical surface [23, 24], due to their productions being mostly at the intermediate stage of collisions and suffering particularly the processes of thermalization and expansion of the interacting system.

4 Conclusions

We summarize here our main observations and conclusions.

(a) We have used the hybrid model to describe the top quark-related spectra of p_T and y, which include the spectra of $t\bar{t}$ systems, hadronic top quarks, and top quarks produced in pp collisions at $\sqrt{s} = 8$ TeV measured by the ATLAS Collaboration at the LHC. The hybrid model uses the superposition of the inverse power-law and the Erlang distribution for the description of p_T spectra and the two-component Gaussian function for the description of y spectra. The inverse power-law, the Erlang distribution, and the two-component Gaussian function are derived from the QCD calculus, the multisource thermal model, and the Landau hydrodynamic model, respectively. We have used the inverse power-law and the Erlang distribution to describe the harder and hard scattering processes respectively.

(b) The modelling results are in agreement with the experimental data of the $t\bar{t}$ systems and the hadronic top quarks measured at the detector level, the fiducial phase-space normalized differential cross-sections for the $t\bar{t}$ systems and the hadronic top quarks, and the full phase-space normalized differential cross-sections for the $t\bar{t}$ systems and the top quarks. The $t\bar{t}$ systems show only the contribution of harder scattering process (with $k = 1$). The (hadronic) top quarks show mainly the

contribution of hard scattering process (with a small k). These render that more collision energies are needed to create the $t\bar{t}$ system. As a part of the $t\bar{t}$ system, the (hadronic) top quark apportioned partly the energy of $t\bar{t}$ system, which results in a not too hard scattering process.

(c) When the experimental requirement changes from the detector level to the fiducial phase-space and then to the full phase-space, for both the $t\bar{t}$ systems and the (hadronic) top quarks, p_0 and n decrease, and y_F and σ_{y_F} increase. Only for the (hadronic) top quarks, k slightly increases, and $\langle p_{Ti}\rangle$ and m almost do not change. Although these tendencies of the parameters may have no obvious meaning due to little relations among these experimental requirements, these parameters can be used in the extraction of discrete values of some kinematic quantities. In fact, based on these parameters, we have obtained some discrete values of the velocity, momentum, and rapidity components. Based on these discrete values, the event patterns in some three-dimensional spaces are obtained.

(d) The event patterns in the three-dimensional β_x-β_y-β_z space for the $t\bar{t}$ systems in the three requirements are rough cylinders with $\sqrt{\overline{\beta_x^2}} \approx \sqrt{\overline{\beta_y^2}} \ll \sqrt{\overline{\beta_z^2}}$ and $|\beta_x|_{\max} \approx |\beta_y|_{\max} < |\beta_z|_{\max}$. The event patterns for the (hadronic) top quarks in the three requirements are rough ellipsoids with the similar relations among these quantities. Both the quantities on the root-mean-squares and the maximums for the $t\bar{t}$ systems are less than those for the (hadronic) top quarks, and the differences in relative sizes between transverse and longitudinal quantities for the $t\bar{t}$ systems are larger than those for the (hadronic) top quarks.

(e) The event patterns in the three-dimensional p_x-p_y-p_z space for the $t\bar{t}$ systems in the three requirements are relative thin and very rough ellipsoids with $\sqrt{\overline{p_x^2}} \approx \sqrt{\overline{p_y^2}} \ll \sqrt{\overline{p_z^2}}$ and $|p_x|_{\max} \approx |p_y|_{\max} \ll |p_z|_{\max}$. The event patterns for the (hadronic) top quarks in the three requirements are relative fat and very rough ellipsoids with the similar relations among these quantities. The transverse quantities for the $t\bar{t}$ systems are less than those for the (hadronic) top quarks, and the situations of longitudinal quantities are opposite. The differences in relative sizes between transverse and longitudinal quantities for the $t\bar{t}$ systems are larger than those for the (hadronic) top quarks. The maximum quantities do not show an obvious tendency for the $t\bar{t}$ systems and the (hadronic) top quarks.

(f) The event patterns in the three-dimensional y_1-y_2-y space for the $t\bar{t}$ systems in the three requirements are very rough ellipsoids with $\sqrt{\overline{y_1^2}} \approx \sqrt{\overline{y_2^2}} \ll \sqrt{\overline{y^2}}$ and $|y_1|_{\max} \approx |y_2|_{\max} \ll |y|_{\max}$. The event patterns for the (hadronic) top quarks in the three requirements are very rough rhombogen with the similar relations among these quantities. Both the quantities on the root-mean-squares and the maximums for the $t\bar{t}$ systems are obviously less than those for the (hadronic) top quarks. The differences in relative sizes between transverse and longitudinal quantities for the $t\bar{t}$ systems are larger than those for the (hadronic) top quarks.

(g) According to these scatter plots, we have obtained the probability distributions of the considered quantities such as β_i, p_i, and y_i. The distributions of x and y components are almost the same, if not equal to each other at the pixel level, due to the assumption of isotropic emission in the transverse plane. β_x and β_y distribute only in a small region near zero. The $t\bar{t}$ systems have a more narrow region and a higher peak than the (hadronic) top quarks. β_z distributes almost uniformly in a wide region for different particles and requirements. In particular, the distributions of $|\beta_z|$ of the (hadronic) top quarks increase slightly with the increase of $|\beta_z|$, while the $t\bar{t}$ systems show an opposite or placid tendency.

(h) All the distributions of p_x, p_y, and p_z for different particles and requirements have a peak at zero, though the distribution of p_z has a wider range and a lower peak than those of p_x and p_y. The $t\bar{t}$ systems have a higher peak in p_x and p_y distributions, while other three types of distributions have severally similar shapes and do not show obviously such a high peak. In the distributions of y_1 and y_2, a higher peak for the $t\bar{t}$ systems than for the (hadronic) top quarks is observed. For the hadronic top quarks, the distributions of y_1 and y_2 at the detector level and in the fiducial phase-space are almost the same, and they are different in shape and slope around the peak region from the distributions for the top quarks.

Conflict of Interests

The authors declare that there is no conflict of interests regarding the publication of this paper.

Acknowledgments

This work was supported by the National Natural Science Foundation of China under Grant No. 11575103 and the US DOE under contract DE-FG02-87ER40331.A008.

References

[1] CDF Collaboration (F. Abe *et al.*), Phys. Rev. D **50**, 2966 (1995).

[2] CDF Collaboration (F. Abe *et al.*), Phys. Rev. Lett. **73**, 225 (1995).

[3] CDF Collaboration (F. Abe *et al.*), Phys. Rev. Lett. **74**, 2626 (1995).

[4] D0 Collaboration (S. Abachi *et al.*), Phys. Rev. Lett. **74**, 2632 (1995).

[5] J.L. Synge, *The Relativistic Gas* (North-Holland, Amsterdam, The Netherlands, 1957).

[6] P.Z. Ning, L. Li, D.F. Min, *Foundation of Nuclear Physics: Nucleons and Nuclei* (Higher Education Press, Beijing, China, 2003).

[7] C.D. Dermer, Astrophys. J. **280**, 328 (1984).

[8] J. Cleymans, D. Worku, Eur. Phys. J. A **48**, 160 (2012).

[9] C. Tsallis, J. Stat. Phys. **52**, 479 (1988).

[10] G. Wilk, Z. Włodarczyk, Eur. Phys. J. A **40**, 299 (2009).

[11] T.S. Biró, Eur. Phys. J. A **40**, 255 (2009).

[12] T.S. Biró, G. Purcsel, K. Ürmössy, Eur. Phys. J. A **40**, 325 (2009).

[13] W.M. Alberico, A. Lavagno, Eur. Phys. J. A **40**, 313 (2009).

[14] H. Zheng, L.L. Zhu, Adv. High Energy Phys. **2016**, 9632126 (2016).

[15] UA1 Collaboration (G. Arnison *et al.*), Phys. Lett. B **118**, 167 (1982).

[16] R. Odorico, Phys. Lett. B **118**, 151 (1982).

[17] M. Biyajima, T. Mizoguchi, N. Suzuki, arXiv:1604.01264 [hep-ph] (2016).

[18] F.-H. Liu, Y.-Q. Gao, T. Tian, B.-C. Li, Eur. Phys. J. A **50**, 94 (2014).

[19] J. Schwinger, Phys. Rev. **82**, 664 (1951).

[20] R.-C. Wang, C.-Y. Wong, Phys. Rev. D **38**, 348 (1988).

[21] C.-Y. Wong, *Introduction to High Energy Heavy Ion Collisions* (World Scientific, Singapore, 1994).

[22] P. Braun-Munzinger, K. Redlich, J. Stachel, in *Quark-Gluon Plasma 3*, edited by R.C. Hwa, X.-N. Wang (World Scientific, Singapore, 2004) arXiv:nucl-th/0304013 (2004).

[23] Y.-H. Chen, G.-X. Zhang, F.-H. Liu, Adv. High Energy Phys. **2015**, 614090 (2015).

[24] Y.-H. Chen, F.-H. Liu, S. Fakhraddin, M.A. Rahim, M.-Y. Duan, arXiv:1607.00488 [hep-ph] (2016).

[25] Y.-H. Chen, F.-H. Liu, R.A. Lacey, Adv. High Energy Phys. **2016**, 9876253 (2016).

[26] L.D. Landau, Izvestiya Akademii Nauk: Series Fizicheskikh **17**, 51 (1953).

[27] S.Z. Belenkij, L.D. Landau, Soviet Physics Uspekhi **56**, 309 (1955).

[28] P.A. Steinberg, Nucl. Phys. A **752**, 423 (2005).

[29] Z.-J. Jiang, H.-P. Deng, Y. Zhang, H.-L. Zhang, Nucl. Phys. Rev. (China) **32**, 398 (2015).

[30] ATLAS Collaboration (G. Aad *et al.*), Eur. Phys. J. C **76**, 538 (2016).